MIXING ANALYSIS OF A SWIRLING RECIRCULATING FLOW USING DNS AND EXPERIMENTAL DATA

Martin Freitag, Markus Klein, Mark Gregor, Andreas Nauert, Dirk Geyer, Christoph Schneider, Andreas Dreizler, Johannes Janicka
Fachgebiet Energie– und Kraftwerkstechnik,
Technische Universitt Darmstadt
Petersenstr. 30, Darmstadt, D–64287, Germany
mfreitag@ekt.tu-darmstadt.de

ABSTRACT

Fluid flow and mixing of a recirculating, swirling flow was investigated by direct numerical simulation (DNS) at a Reynolds number of $Re = 5000$. Its accuracy was assessed by grid refinement studies and also by comparing the results to experimental velocity data obtained by laser Doppler velocimetry (LDV). The mixing field was investigated experimentally using spontaneous Raman-scattering and planar laser induced fluorescence (PLIF). Detailed one point statistics will be presented and discussed. In addition a comparison between two point statistics of the velocity and the scalar field will be given. Further on, the impact of a precessing vortex core (PVC) on the mixing process will be examined.

The database will be used in the future for testing 1.) a newly developed model for the turbulent scalar flux (see Klein et al. 2004), as well as 2.) strategies for assessing the quality of large eddy simulations.

INTRODUCTION

Fluid-mixing by turbulent motion is of great importance for processes such as heat and mass transfer or chemical reaction. The effect of swirl can enhance mixing drastically and also it can be used to stabilize premixed flames in an inherent way. Therefore, the prediction methods used for this type of flows - like RANS, URANS and LES - must be assessed in their quality. For this purpose, direct numerical simulations (DNS) can be performed at moderate Reynolds numbers to create a database for quality assurance and also to provide comprehensive information to scientists and engineers.

The investigation of swirl flows, experimentally as numerically, in a wide range of Reynolds numbers has been an ongoing effort during the last fifty years. Detailed description on the phenomena of vortex breakdown caused by swirling motion can be found in Syred and Beer (1972) or Fahler and Leibovich (1977). Recently, a large bandwidth of publications within this subject has been summarized in the review of Lucca-Negro and O'Doherty (2000). Initially Chanaud (1965) documented a coherent structure of vortex type, performing a precessing motion (precessing vortex core, PVC), which has been observed to occur in isothermal flows, premixed and non premixed combustion. If the investigated swirl flow is running under premixed combustion conditions, the coherent structure can cause a feedback mechanism with acoustic modes, resulting into back-stroke of the flame into the nozzle.

DNS of a swirling jet at ($Re = 200$) was used to investigate the phenomena of vortex breakdown, with different aspects (Ruith et al., 2003). Also the authors compared different visualization techniques, considering the question, if they really identify the PVC or only the turbulent shear stresses. Freitag et al. (2004) studied a turbulent swirling flow by means of a DNS and characterised the flow field in terms of one and two point statistics. The precessing vortex core was quantified using frequency analysis and spatial two point correlations.

The considerable progress in the application of the large eddy simulation (LES) approach to increasingly complex geometries can be found also in various publications on swirl flows. Exemplary we like to mention the excellent results with swirled coaxial jets (Pierce and Moin, 1998), who also predict a scalar concentration. Promising results of an isothermal swirl flow with recirculation have been published by Tang et al. (2002). Wegner et al. (2004) documented LES and URANS of the same geometry.

In order to develop better modeling strategies for such flows, going beyond the gradient flux approximation with its well known deficiencies, corresponding DNS data would be highly desirable. But direct simulations including scalar transport so far were mostly performed for relatively simple configurations (see e.g. Hattori et al. 2003; Kim and Moin 1989; Klein et al. 2004).

This paper presents an first attempt in setting up a DNS database of more complex configurations, and will be used in the future for testing 1.) a newly developed model for the turbulent scalar flux (see Klein et al. 2004), as well as 2.) strategies for assessing the quality of large eddy simulations.

SETUP AND MEASUREMENT TECHNIQUE

The experimental setup consists of a movable block type swirler, which feeds an annulus from where the airflow enters the measurement section at ambient pressure and temperature. The Reynolds number was calculated from the bulk velocity and the bluff-body diameter. The geometrical swirl number was set to S=0.75. A coflow of 0.5 m/s surrounds the swirler device. More details can be taken from Schneider et al. (2005) and Freitag et al. (2004).

Transient velocities have been measured by two-dimensional LDV in back scatter mode. A mixture of MgO and $ZrSiO_4$ served as seeding material. Along axial and various radial profiles statistical moments have been deduced from about 10000 independent events per measurement point. Additionally, auto-correlations were deduced from time-series using the fuzzy slotting technique, local normalization, and transit time weighting (Maanen et al., 1999). Respective time

scales and power spectra have been estimated by integration and Fourier transformation, respectively.

Mixing fields were determined by one-dimensional Raman scattering and PLIF. As passive scalar either methane (5vol.% in air, Raman scattering) or acetone (5mass.% in air, PLIF) was used. These two tracers differ in density. By comparing results from such tracers the influence of the tracer choice on the mixing field can be examined experimentally. Notice, that in an ongoing effort propane is going to be investigated by Raman scattering to avoid a possible bias by two different measurement techniques.

For Raman scattering a cluster of four quality-switched frequency-doubled Nd:YAG lasers in addition with an optical delay line served to deliver a pulse train approximately 350 ns long containing an energy of 1.2 J. The measurement volume extended 5.6 mm in direction of the laser beam pointing. Ro-vibrational Raman bands of CH_4, N_2 and O_2 were imaged perpendicularly onto a slit of a Czerny-Turner type spectrometer by means of a custom-designed achromatic corrected f#=2 lens system (Geyer et al., 2004). Raman spectra were recorded by a thermo-electrically cooled backside illuminated CCD camera with low noise. The camera read-out time limited the repetition rate to approximately 1 Hz. To allow for single-shot measurements the CCD detector was gated by an ultra-fast mechanical shutter assembly (10 μs long gates). Binning in spatial direction resulted in 16 adjacent measurement "points" along the 1D measurement volume with a spatial resolution 400x400x400 μm^3 each. Data evaluation of single-shot measurements was based on spectral fitting of theoretical Raman spectra (Geyer and Dreizler, 2004) to experimental spectra delivering transient local mixing of the passive scalar. Using 600 single-shots at each measurement location, the first two statistical moments were extracted from the data. The precision of mean mixture fraction was 0.7%. Radial profiles were recorded at axial heights of 10, 20, 30, 60, and 90 mm.

In case of PLIF, acetone was excited electronically using a KrF excimer laser operating at 248 nm. Pulse length and energy were 20 ns and 150 mJ, respectively. The exciting laser light sheet extended 17 mm in axial direction and was focused by a single f=200 mm cylindrical lens into the measurement plane. The beam waist was 180 μm thick and was released at r=30 mm. Fluorescence was detected perpendicular to the laser pointing by means of a gated intensified CCD camera. The read-out times limited the overall repetition rate to 1 Hz. Fluorescence images were normalised on laser beam profile, pulse energy and relative acetone concentration. Median filtering (3x3 pixel) resulted in a spatial resolution in the image plane of 150 x150 μm. Transient local acetone concentrations were deduced from relative fluorescence intensities. In accordance to the Raman data evaluation so far only the first two statistical moments were deduced from the data. The noise was dominated by photon noise and was estimated to equal 10%, for the first moment. PLIF images were taken at different axial heights. The planes were centered axially downstream at x=8.5, 30.5, and 60.5 mm. At each height 1000 single-shots were taken.

NUMERICAL TECHNIQUE AND CONFIGURATION

The governing equations for the investigated problem are the conservation equations of mass and momentum for an incompressible Newtonian Fluid in their instantaneous local form, as well as a transport equation for a passive scalar. The molecular diffusion coefficient of the scalar transport equation, is expressed by the ratio of kinematic viscosity and the Schmidt number (Sc), which was set to 0.74 in the calculation, to match the experimental Schmidt number. The variables are located on a staggered, cylindrical grid, where the passive scalar F and the pressure are stored at the cell center. All equations are solved by using a finite volume technique. For spatial discretization second order central differences are used for the momentum equation. The convective fluxes of the scalar equation are discretized using a nonlinear TVD-limiter-scheme (CHARM) (PHOENICS, 2002), to keep the solution bounded, and to avoid unphysical oscillations in the concentration field. Temporal discretization is an explicit third order Runge-Kutta-method and the Poisson equation is inverted by using a direct fast elliptic solver.

To allow recirculating fluid entering the nozzle, at least part of the nozzle has to be included in the computational domain. Due to the fact that the solver is of single block structure, immersed boundaries Saiki and Biringen (1996) are used to mimic the nozzle. Hereby, the walls of the nozzle are expressed by an artificial force added to the momentum equation. This force has been calculated according to

$$f(x,t) = \alpha \int_0^t U(x,t)\, dt' + \beta U(x,t) \qquad (1)$$

where $\alpha = -100.0$ and $\beta = -0.9725$ have been chosen to be negative constants. The force has been added to the velocities after the pressure correction at every Runge-Kutta time step.

The computational domain, $12D$ axial (x) and $8D$ radial (r) is resolved with $720 \times 256 \times 240$ ($\approx 44.23 \cdot 10^6$) grid nodes, where axially 2D are allocated to the nozzle extension. Except for the inflow boundary the domain is open at all other boundaries. Neumann boundary conditions for the velocity and the pressure are prescribed at the outflow, negative velocities are clipped. At the encompassing boundaries, velocities are treated with Neumann conditions and the pressure is set to be equal zero witch allows mass entrainment. A developed channel velocity profile, with constant tangential velocity and superimposed pseudo turbulent fluctuations are used as inflow conditions down the nozzle, more details about the method and its application can be taken from Klein et al. (2003a) and Klein et al. (2003b). The ratio of axial and tangential velocity was chosen to match the experimentally determined swirl number ($S = 0.64$). A co-axial air flow of $0.5 m/s$ surrounds the swirler device.

The simulation as well as the experimental investigation of the scalar concentration was carried out at a Reynolds number of 5000. In contrast the transient velocity information has been taken from experiments running at $Re = 10000$. In order to compare this data with the DNS, the experimental data was scaled with the ratio of the corresponding Reynolds numbers. The applicability of this procedure is given, because the profiles have been found to collapse if normalized with the corresponding bulk velocity (Schneider et al., 2005) and (Freitag et al., 2004).

The simulation run 40000 time steps on four processors, which corresponds to 8 flow through times in terms of the bulk velocity, so the number of collected samples can been considered as sufficient.

RESULTS AND DISCUSSION

In this section the radial velocity profiles as well as the turbulent kinetic energy will be presented to assess the quality of the DNS velocity data. Secondly, statistical data of the scalar mixing will be compared to experimental findings and discussed. Also a visualization of the mixing will be given. Further on, two point statistics will be compared with experimental findings. The section will be closed by a discussion, how the precessing vortex core influences the mixing process.

Velocity Profiles

As a consequence of the relatively high swirl number an internal recirculation zone is generated by vortex breakdown. A further consequence is the appearance of a fluid dynamic instability called precessing vortex core.

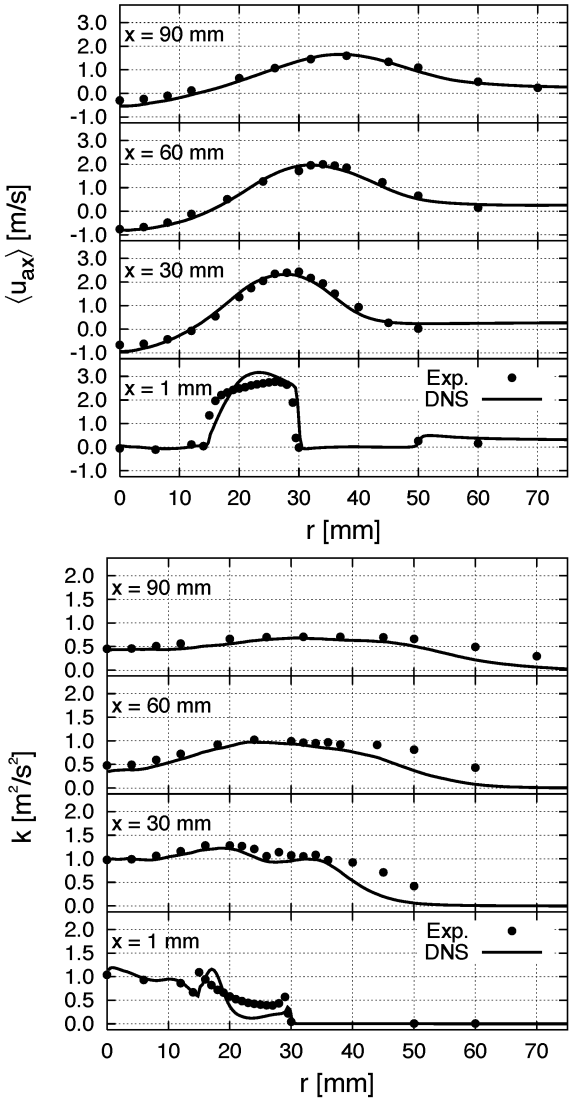

Figure 1: Radial plots of the mean axial velocity and of the turbulent kinetic energy for selected axial positions

Exemplarily figure 1 shows radial profiles of the mean axial velocity and the turbulent kinetic energy at different axial positions. The agreement of the simulated data with experimental data is excellent, except for a moderate under-prediction of the TKE for large radii. Also the length of the recirculation zone is well predicted as the plots of the axial velocity indicate. The high values of the turbulent kinetic energy at the axis of symmetry at x=1mm and x=30mm are due to the the precessing motion of the coherent structure.

Other features of the flow are high shear stress at the inner and outer edges of the annular flow issuing from the slit and a spreading of the flow pattern typical for these swirling flows.

Scalar concentration

To get a first impression about the mixing a 2D snapshot - of the DNS - showing iso surfaces, representing 95%, 50% and 25% concentration levels, is given in picture 2. Due to the strong recirculation a very large region above the nozzle consists of fluid at medium concentration.

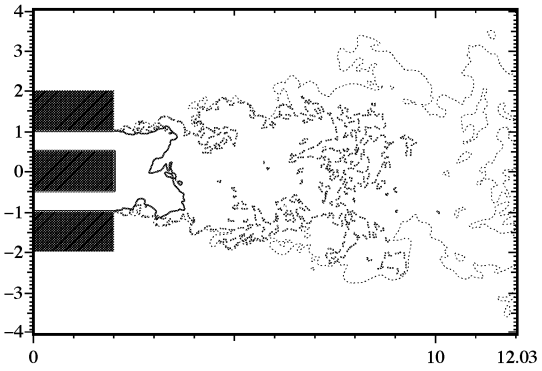

Figure 2: Instantaneous snapshot of iso-levels, representing 95%, 50% and 20% concentration.

First and second order statistics of the scalar field have been calculated to evaluate the mixing behavior of the swirl flow. Results of the comparison between the DNS calculation, Raman scattering and PLIF statistics can be found in figures 3 and 4. The DNS and the Raman results exhibit an overall good agreement, in contrast to the acetone PLIF measurements. First of all we would like to discuss the DNS and the Raman data, and disregard the acetone tracer PLIF, where we will focus on later.

The agreement of mean quantities between the calculation and the Raman measurements is very good, and also the agreement in terms of fluctuations is reasonable, considering the complexity of the flow. The underprediction of the fluctuation intensity for large radii is consistent with the before mentioned underprediction of TKE. Using a Boussinesq assumption this can explain the sligthly larger spreading of the mean scalar due to a increased turbulent transport observed in the experiment.

The large deviation between results from PLIF and the other techniques, especially at $30mm$ and $60mm$, derive from the used tracer, the low Reynolds number and the vertical adjustment of the experiment. Due to the fact that acetone is twice the density of the surrounding air, the mixture is very likely to decompose. Within regions, where the axial momentum is small, the counter directed gravity tends to drag the acetone backwards. This results in the formation of large acetone clouds in the environment of the measurement section. A snapshot of the acetone concentration is presented in figure 5 directly above the nozzle. The physical dimension of the box

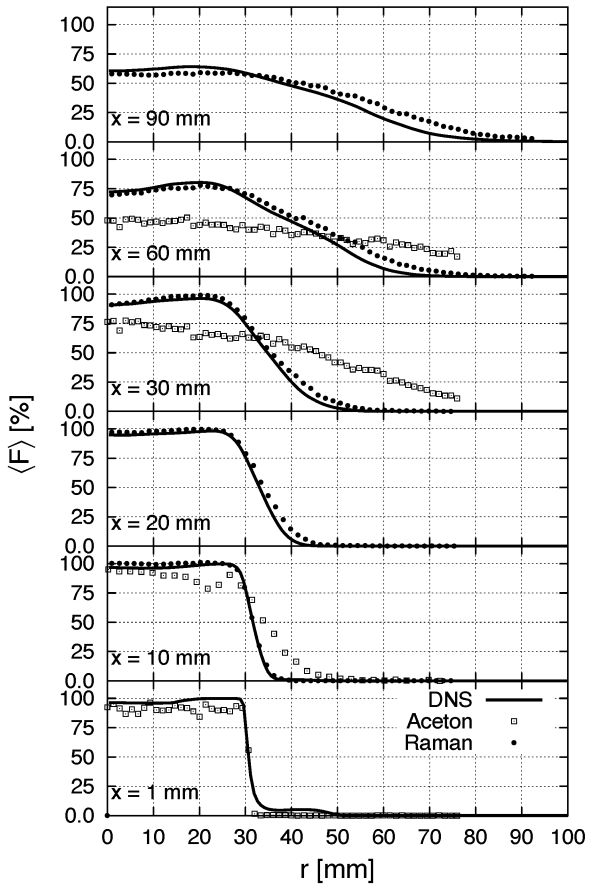

Figure 3: Radial plots of the mean of the passive scalar for different axial positions

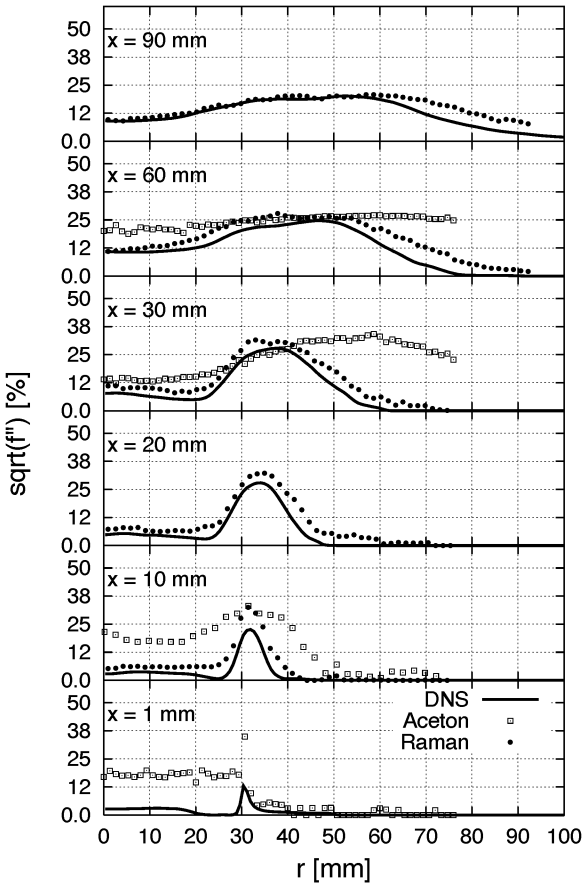

Figure 4: Radial plots of the fluctuation of the scalar concentration for different axial positions

is 14mm in height (axial) and 30mm in width (radial). The lines represent iso surfaces of the DNS, between 95% and 25% concentration. Parts of the described acetone clouds can be identified at he upper right side of the picture, a region, where both Raman and DNS never found any concentration of the passive scalar.

The high fluctuations, observed in the PLIF data, of about 20% at $1mm$ and $10mm$, even though the mean value is nearly 100%, can be explained with the normalization of the profiles. Driven by the relatively high swirl number, recirculating fluid enters the nozzle and transports additional acetone into the nozzle. Therefore the average concentration of acetone exiting the nozzle can be larger then the theoretical maximum. To account for this effect the data was normalized on a single-shot base. For this purpose an accumulated intensity along a $4mm$ heigh and $30mm$ wide strip centered at $20mm$ was used.

Because the DNS is undertaken under the assumption that the scalar is strictly passive and of the same density as air, naturally gravity effects can not be captured. It is worth to mention that even if the simulation would include the difference in density a decomposition of mixture is almost impossible to handle without applying additional modeling.

To identify the density variation as the decisive reason for the variation between the experimental data and the DNS results, two main efforts were undertaken. Experimentally a higher Reynolds number $Re = 40000$ was investigated, to minimize the influence of gravity. The tendency to show better results was given at an axial height of $10mm$ and $20mm$ but far downstream the same stagnating acetone cloud was formed. Numerically large eddy simulations of different density ratios $\rho/\rho_0 = 1.0, 1.1, 1.25$ were performed. It was observed that even at a small density ratio of 1.1 which represents the density variation of environmental air to the acetone/air mixture, an acetone cloud forms up. This cloud stagnates for a very short time, before it moves backwards and fills the complete calculation domain.

Figure 5: Acetone concentration image, together with iso surfaces taken from the DNS (95%, 50%, 20%) representing the concentration. A cloud of the heavy acetone-mixture stagnates at the upper right edge of the picture.

Considering all this facts the capability of acetone as tracer in low Reynolds number air flows is questionable, due to the relatively high density gradient. Also at higher Reynolds numbers this effect can occur locally, where the convection is small in contrast to volume forces.

Two Point Statistics

In addition to statistical moments two point velocity correlations with radial and axial separation have been evaluated at different positions in the flow and will be compared in this section to two point LDV measurements. The correlation functions are normalized and plotted against the separation distance normalized with the axial position as in Schneider et al. (2005) (see figure 6). Although both data sets still contain some statistical noise, the agreement with the experimental results is satisfactory.

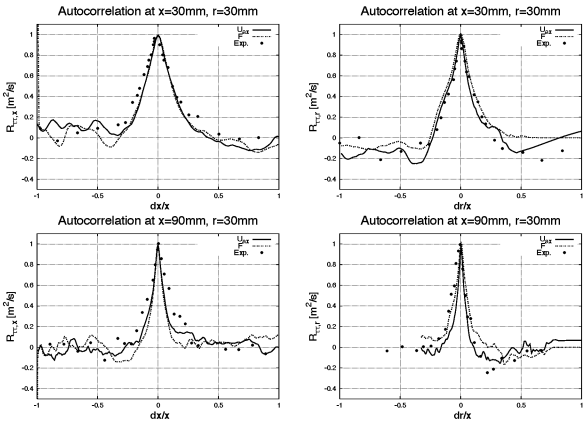

Figure 6: Two point correlations, taken from the axial velocity and the mixture, at two positions ($30mm$ and $90mm$ downstream and $30mm$ from the centerline), in comparison with experimental data.

By comparing the correlations at different axial positions it can be observed as a general feature that the axial length scales do not enlarge uniformly downstream, as typical in jet configurations. In that case the correlation functions would collapse, when normalized with the axial distance from the nozzle.

Additional to the velocity, two point correlations of the mixture fraction have been evaluated from the DNS, see figure 6. They show the same features as observed for the velocity two point correlations: Except for the last axial position (90mm), the correlations are asymmetric with respect to the point of zero separation and they show strong undershoots and oscillations (especially for smaller radii not shown here). Furthermore, by visual inspection the ratio of longitudinal and transverse length scale seems to be different from a ratio of 2.0 as expected for isotropic turbulence. It is also planned to extract according respective information from the Raman measurements.

Impact of the coherent structure

As the PVC stabilizes, the precession frequency can be obtained from the temporal autocorrelation of the velocities, pressure or the transported scalar. Figure 7 shows the spectra of the autocorrelation computed from the axial velocity at $x = 30mm$ and $20mm$ away from the centerline and from the mixture concentration, at the same position. Clearly both spectra show a dominant reiterate characteristic, which arises as a peak in the computed frequency spectra at 21Hz.

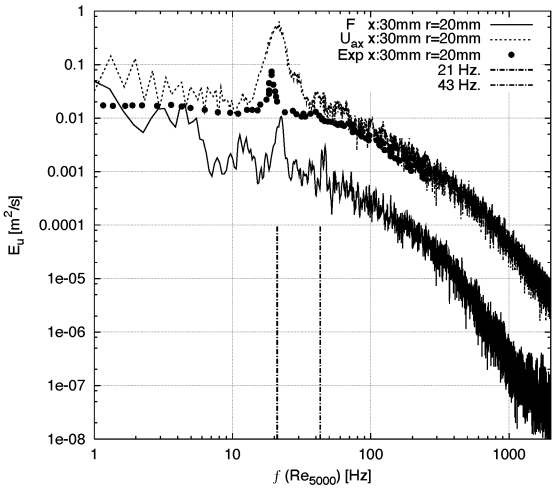

Figure 7: Energy-density spectra of the passive scalar and of the axial velocity at a characteristic positions shows the frequency of the rotating structure. The experimental energy-density spectra of the axial velocity is scaled to match the Reynolds number.

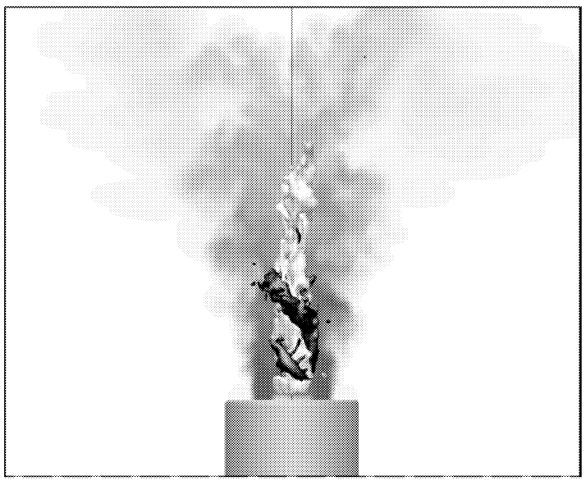

Figure 8: 3D plot of the pressure iso-surface to visualize the structure of the PVC (black), which wraps around the recirculating fluid (white), cutting a projection of the scalar concentration (dark grey represents high concentration)

From this absolute frequency the Strouhal number $St \approx L \cdot f/U$ is calculated to compare the results with the experimental data. Taking the bluff body diameter as L and the mean bulk velocity for U we obtain a Strouhal number of $St \approx 0.27$, very close to the value of 0.25 found in the experimental investigations of Schneider et al. (2005) at Re=10000. Due to the low repetition rate of the spontaneous Raman measurements (1Hz) time dependent data could not be extracted. Because of the impact of the precessing vortex core,

it is not surprisingly that the frequency can also be found in the mixture concentration. It can be observed that the PVC sucks surrounding air into the spreading cone of the flow, and thereby enhances the mixing process.

In figure 8 the coherent structure of the PVC is visualized using an iso-surface of the pressure-field ($P = P_0 - 0.25$, black shape). The recirculation zone is presented by an iso-surface of negative axial velocity (white). The scalar concentration is plotted on a plane, where dark grey represents high values and light grey low concentrations. Clearly the helical structure of the PVC can be observed. From classical vortex breakdown investigations as documented in Syred and Beer (1972) or Lucca-Negro and O'Doherty (2000) the PVC is described to encase the recirculation zone, also nicely visible in figure 8.

CONCLUSIONS

A DNS of a swirling recirculating flow has been performed, taking into account the transport of a passive scalar. The same configuration has been investigated experimentally at our in house facilities using LDV, acetone PLIF and Raman scattering. The present results demonstrate that the numerical scheme represents the flow field of this highly complex configuration very well. The mixing field is in good agreement with experimental data. Detailed statistical results, including one point statistics, two point correlations and time series are included in an established database, which will be used to enhance the understanding of such complex flows.

ACKNOWLEDGEMENTS

The authors gratefully acknowledge the financial support by the DFG SFB 568 (project B1, B3 and D3) and also the DFG project Dr374/4-1.

REFERENCES

R. Chanaud. Observation of oscillatory motion in centain swirling flows. *J. Fluid. Mech.*, 21:111–127, 1965.

J. Fahler and S. Leibovich. Disrupted states of vortex flow and vortex breakdown. *Phys Fluids*, 20:1385–1400, 1977.

M. Freitag, M. Klein, and J. Janicka. Direct numerical simulation of a recirculating, swirling flow. In *2nd International Workshop on Trends in Numerical and Physical Modelling for Turbulent Processes in Gas Turbine Combustors*, Darmstadt, 2004.

D. Geyer and A. Dreizler. Evaluation of raman scattering experiments in hydrocarbon flames. In *Proc. Laser Applications to Chemical and Environmental Analysis*, 2004.

D. Geyer, A. Kempf, A. Dreizler, and J. Janicka. Scalar dissipation rates in isothermal and reactive turbulent opposed jets: 1d-raman/rayleigh experiments supported by les. *Proc. Combust. Inst.*, 30:681–689, 2004.

H. Hattori, Y. Murase, and Y. Nagano. Dns of turbulent heat transfer in plane impigning jet. In K. Hanjalic, Y. Nagano, and M. Tummers, editors, *Proceedings of Turbulence, Heat and Mass Transfer 4*, pages 449–456, 2003.

J. Kim and P. Moin. Transport of passive scalars in turbulent channel flow. In *Turbulent Shear Flow VI*, page 85. Springer Verlag, 1989.

M. Klein, A. Kempf, A. Sadiki, and J. Janicka. Mixing analysis of a plane jet using direct numerical simulation. In *Euromech 10th European Turbulence Conference*, Trondheim, Norway, July 2004.

M. Klein, A. Sadiki, and J. Janicka. A digital filter based generation of inflow data for spatially developing direct numerical or large eddy simulations. *J. Comp. Physics*, 186: 652–665, 2003a.

M. Klein, A. Sadiki, and J. Janicka. Investigation of the influence of the reynoldsnumber on a plane jet using direct numerical simulation. *International Journal of Heat and Fluid Flow*, 24/6:785–794, 2003b.

O. Lucca-Negro and T. O'Doherty. Vortex breakdown: a review. *Progress in Energy and Combustion Science*, 27: 431–481, 2000.

H. V. Maanen, H. Nobach, and L. Benedict. Improved estimator for the slotted autocorellation function for randomly sampled ldv data. *Meas. Sci. Tech.*, 10:L4–L7, 1999.

PHOENICS. *www.cham.co.uk/phoenics/d_polis /d_lecs/numerics/scheme.htm. WWW*, 2002.

C. Pierce and P. Moin. Large eddy simulation of a confined coaxial jet with swirl and heat release. *AIAA*, 98(2892): 1–11, 1998.

M. Ruith, P. Chen, E. Meiburg, and T. Maxworthy. Three-dimensional vortex breakdown in swirling jets and wakes: direct numerical simulation. *J. Fluid. Mech.*, 486:331–378, 2003.

E. Saiki and S. Biringen. Numerical simulation of a cylinder in uniform flow: Application of a virtual boundary method. *J. Comp. Phys*, (123):2:450–465, 1996.

S. Schneider, A. Dreizler, and J. Janicka. Fluid dynamical analysis of atmospheric reacting and isothermal swirling flows. *Flow Turbulence and Combustion*, submitted, 2005.

N. Syred and J. Beer. The damping of precessing vortex cores by combustion in swirl generators. *Acta Astronautica*, 17: 783–801, 1972.

G. Tang, Z. Yang, and J. McGuirk. Large eddy simulation of isothermal confined swirling flow with recirculation. *Engineering Turbulence Modelling and Experiments*, 5:885–894, 2002.

B. Wegner, A. Maltsev, C. Schneider, A. Sadiki, A. Dreizler, and J. Janicka. Assesment of unsteady rans in predicting swirl flow instability based on les. *International Journal for Heat and Fluid Flow*, 25:528–536, 2004.